Adaptive Active Contours for the 3D Segmentation of Computed Tomography Images

Miguel Alemán-Flores and Luis Alvarez
Departamento de Informática y Sistemas
Universidad de Las Palmas de Gran Canaria
Las Palmas, Spain
Email: {maleman, lalvarez}@dis.ulpgc.es

***Abstract*—Computed Tomography is one of the most valuable modalities of medical imaging and is used in the diagnosis of a wide range of pathologies. In many cases, it is necessary to obtain a precise segmentation and a 3D visualization of certain organs, tissues, nodules or regions in the tomography. However, manual delimitation is a very time-consuming process and advanced applications are needed to perform this process automatically. Active contours intend to fit an initial approximation to the most relevant edges around the starting contour. Most approaches of active contours assume that all points in the initial approximation are close to the final solution and that similar conditions can be set to all the sections of the contour, which is frequently a false assumption. For that reason, we have developed a new approach, in which different terms are used and adapted according to the evolution of the contour. Balloon, regularizing and attraction terms are combined and extended to 3D, avoiding the need for a close initial approximation and reducing human intervention. Furthermore, a multiscale framework is added to tackle the heterogeneity of the images and the variability of the approximations. The combination of these terms allows obtaining a more precise segmentation of the tomography.**

***Keywords*—segmentation; computed tomography; active contours.**

I. INTRODUCTION

Computed tomography (CT) is a medical imaging technique which generates tomographic images or slices from computer-processed X-rays. The cross-sectional images which are obtained can be used for diagnostic and therapeutic purposes. For an appropriate assessment of a radiological study, or for the extraction of certain measurements, the segmentation of the corresponding organs, tissues, or regions is frequently needed.

Different approaches have been proposed to perform this kind of segmentations, from graph-based algorithms [1] to atlas-based systems [2] and region-growing schemes [3]. Some methods are fully automated [4], some others require human intervention [5].

Active contours are a very useful tool for adjusting a contour to the edges in an image [6][7][8]. The basic idea underlying active contours consists in making a contour evolve locally according to certain features of the neighborhood of each contour point. Several problems arise when applying this technique to computed tomography. First, an initial approximation is required, but manual initialization is an extremely time-consuming task, since each 3D image consists of a large amount of 2D images. Second, these images present noise, heterogeneities and blurred edges, which makes it necessary to include additional terms to separate regions without clearly defined edges. Finally, local minima may stop the evolution on wrong edges.

Some variations have been proposed to tackle these problems in different types of images, but handling all of them is still a challenging task. Among these works, we can find some approaches applied to textured regions and areas without clearly defined edges, using region descriptors or statistical information [9][10][11][12][13]. If we focus on medical images, similar approaches using texture descriptors and statistical information have been applied in [14][15]. Active contours have also been used to deal with other kinds of problems, such as object tracking and motion estimation [16] or tensor images [17].

In this work, we propose a multistage approach in which human intervention has been considerably reduced. First, we filter the images by means of a 3D anisotropic filter. We adapt the ideas of the classical Perona-Malik equation [18] to the diffusion of computed tomographies. Afterward, an initial approximation is obtained from a single inner point of the region we want to segment by combining some terms in the active contours approach. These terms include balloon forces to expand the region, regularizing terms to smooth the contour and include small holes, and attraction terms to fit the contour to the edges. Finally, we introduce a multiscale framework to refine the segmentation and adapt it to the edges in the image. To tackle the problem of irregular edges and variable distance from the initial segmentation to the actual contour, this framework includes different scales in the attraction term, so that the diffusion depends on the magnitude of the gradient in the region. These multiscale active contours allow a better adaptation to the particular features of each area.

This paper is organized as follows: Section II introduces the underlying ideas of active contours and the classical approach used in their application. In Section III, the 3D anisotropic filtering is presented. The three types of morphological active contours (balloon, regularizing and attraction terms) which are combined in this work are presented in Section IV, whereas the multiscale approach used to improve the segmentation is explained in Section V. Section VI explains the post-processing of the 3D contour points to obtain the final volume and Section VII summarizes our main conclusions and future work.

Copyright (c) IARIA, 2013. ISBN: 978-1-61208-310-0

II. Geodesic Active Contours

Geodesic active contours, also known as snakes, are based on the minimization of the following energy with respect to the contour C:

$$E_{gac}(C) = \int_C g_\sigma(C(s))\, ds, \tag{1}$$

where $C : [0, L] \to \mathbb{R}^2$, $L > 0$, is a rectifiable curve parameterized by arc-length s, and ds denotes the arc-length element. The function $g_\sigma(x, y)$ is used to stop the evolution of the snake when it approaches the edges. It is a smooth decreasing function of the modulus of the gradient of a regularized version of the image $I(x, y)$ on which the segmentation is performed, and acts as an edge detector. As in [7], we can use:

$$g_\sigma\left(I\right) = \frac{1}{\sqrt{1 + \alpha \left\|\nabla I_\sigma\right\|^2}}, \tag{2}$$

where I_σ represents the convolution of the original image I with a Gaussian kernel with standard deviation σ. The parameter α controls how contrasted the edges must be to stop the evolution. On the other hand, σ determines how much I is smoothed, so that increasing its value will blur the image, reducing noise but also details. To minimize the energy in (1), we can use a gradient descent curve evolution written as:

$$C_t = -\frac{\delta E_{gac}(C)}{\delta C}, \tag{3}$$

where $\frac{\delta E_{gac}(C)}{\delta C}$ represents the first variation of E_{gac}. Computing the first variation of E, we obtain (see [7]) the curve evolution equation:

$$C_t = (\kappa g_\sigma - \langle \nabla g_\sigma, \mathbf{n} \rangle)\mathbf{n}, \tag{4}$$

where κ denotes the curvature of C. To write the level set formulation of (4), we introduce a function $u(t, x, y)$ as an implicit representation of $C(t)$. Usually, to construct the initial snake $u(0, x, y)$, a set of points determining a parameterization of a polygon $P_0(\tilde{s}) = (x_0(\tilde{s}), y_0(\tilde{s}))$ are manually selected. Afterward, $u(0, x, y)$ is defined in such a way that $P_0(\tilde{s})$ corresponds to the zero level set of $u(0, x, y)$. In our case, instead of manually defining $P_0(\tilde{s})$ by means of several points outlining the contour, we apply the morphological snakes described in Section IV from a single inner point (manually selected by the user) and consider the curve $P_i(\tilde{s})$ obtained when finishing the process. This way, we can define $u(0, x, y)$ as the signed distance function to $P_i(\tilde{s})$ (positive inside, negative outside), or simply consider two different values for the inner and outer regions.

With this approach, the level set formulation of the geometric curve evolution in (4) is given by:

$$\frac{\partial u}{\partial t} = \left\|\nabla u\right\| \operatorname{div}\left(g_\sigma\left(I\right) \frac{\nabla u}{\left\|\nabla u\right\|}\right). \tag{5}$$

If we expand this equation, we obtain the following expression, in which the first term controls the smoothness of the contour and the second one makes the contour evolve toward the highest gradients:

$$\frac{\partial u}{\partial t} = g_\sigma\left(I\right) \left\|\nabla u\right\| \operatorname{div}\left(\frac{\nabla u}{\left\|\nabla u\right\|}\right) + \lambda \nabla u \nabla g_\sigma\left(I\right). \tag{6}$$

The parameter $\lambda > 0$ has been introduced to balance the contribution of both terms. If we increase the value of λ, the attraction term will have a higher contribution and the contour will try to fit to the highest gradients in the current configuration. On the other hand, decreasing its value will round the contour, making it tend to a more regular outline. When an initial approximation is available, geodesic active contours permit to improve the pre-segmentation, since the contour adapts to the minimum of the energy in (1). As mentioned above, this pre-segmentation must be relatively close to the real contour of the region to segment. Otherwise, the effect of the second term in (6) will not be enough to overcome the regularizing effect of the first term and, instead of approaching the real edges, the snake will be rounded and will tend to reduce.

From this general scheme of active contours, we propose a three-stage process to segment the computed tomography images. First, the tomography is filtered using an anisotropic 3D filter. Second, three types of morphological operations are combined to obtain an initial approximation of the contours. Finally, a multiscale scheme for active contours is introduced to refine the approximation and improve its accuracy.

III. Three-Dimensional Anisotropic Filtering

Balloon forces allow obtaining an initial approximation from a seed point, but they need a relatively homogeneous region to expand, in which irrelevant or spurious edges have been removed or reduced. With the aim of reducing noise, but preserving the edges, we first apply a 3D adaptation of Perona-Malik filtering [18]:

$$u_t = div\left(k\left(\left\|\nabla u\right\|\right) \nabla u\right), \tag{7}$$

where we use:

$$k\left(x\right) = e^{-\beta x}. \tag{8}$$

This kind of approaches, which diffuse the image but preserve the most important edges, are usually applied to single 2D images. However, as we deal with a series of uniformly spaced images, we can apply them in three dimensions, so that the noise reduction process also takes into account the neighbors in the previous and next images in the CT, i.e., the values at the same position in the neighboring images. Since the distance between two consecutive images may not be the same as the distance between the pixels within an image, different weights can be assigned to the neighbors in the different coordinates. This way, we filter the 3D image as a whole, and not each slice separately.

Depending on the similarity of the various elements in the 3D image, their contrast and texture, the value of β in (8) can be adapted, as well as the number of iterations in the following discrete approach:

Copyright (c) IARIA, 2013. ISBN: 978-1-61208-310-0

$$u_{i,j,k}^{n+1} = u_{i,j,k}^{n} + \frac{dt}{2\left(dh\right)^{2}} M\left(u_{i,j,k}^{n}\right), \tag{9}$$

where $M\left(u_{i,j,k}^{n}\right)$ is the result of convolving at each point (i,j,k) in the iteration n with the $3 \times 3 \times 3$ mask whose coefficients are:

$$\begin{aligned} C_{i+a,j,k} &= k_{i+a,j,k} + k_{i,j,k} \\ C_{i,j+a,k} &= k_{i,j+a,k} + k_{i,j,k} \\ C_{i,j,k+a} &= k_{i,j,k+a} + k_{i,j,k} \\ C_{i,j,k} &= -k_{i+1,j,k} - k_{i-1,j,k} - k_{i,j+1,k} \\ &-k_{i,j-1,k} - k_{i,j,k+1} - k_{i,j,k-1} - 6k_{i,j,k} \end{aligned} \tag{10}$$

and $a \in \{-1, 1\}$. The values of $k_{i,j,k}$ are obtained from (8) as follows:

$$k_{i,j,k} = e^{-\beta \|\nabla u\|_{i,j,k}}. \tag{11}$$

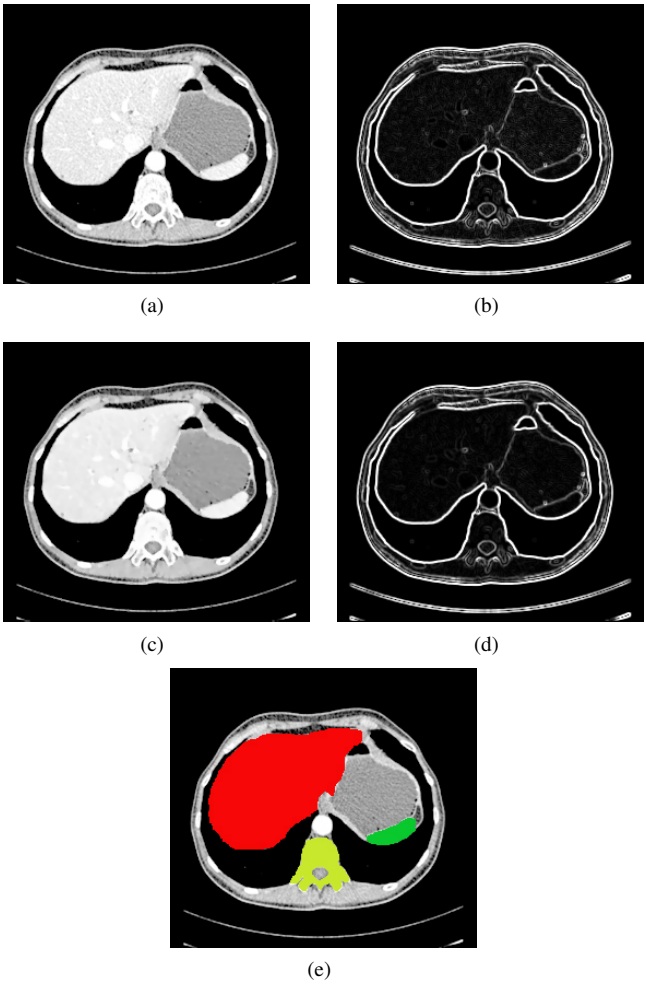

(a) (b) (c) (d) (e)

Figure 1. Image filtering: (a) sample slice of a CT, (b) gradient obtained from the original image, (c) result of the 3D anisotropic filter, (d) gradient obtained from the filtered image, (e) manually delimited regions corresponding to the liver (red), the spleen (green) and a vertebra (yellow).

An increase of β preserves more edges, but also noise. Therefore, its value must be adapted to the amount of noise present in the image and the relevance of the edges to be considered.

Figure 1 shows a slice of the result of applying this type of filter to a computed tomography of the abdominal region. As observed, the edges which are obtained from the filtered image are clearer, which makes them more suitable for a semi-automatic process. Noise and irrelevant edges have been reduced and the morphological snakes can act faster and more precisely to approach the actual edges.

IV. Morphological Snakes

The extraction of the initial approximation is one of the most important drawbacks of active contours. Manual delimitation is extremely time-consuming, even more when dealing with 3D images, as in our case. In particular, when working with large series of images in a computed tomography, it is almost unfeasible and hardly reproducible. As an example, in Figure 1(e), the regions corresponding to the liver, the spleen and a vertebra have manually been delimited. This corresponds to a single image from a large series of two-dimensional images contained in a three-dimensional CT scan. The use of region-growing algorithms is too risky when the limits are not clearly defined. This is the reason why, in order to obtain an initial pre-segmentation from a single point, we use a combination of different morphological operators based on [19][20]. These filters have been extended to three dimensions and applied considering the whole tomography. Instead of adopting the classical level-set approach with a range of values and a limit to separate the inner and outer regions, we work with only two values, so that the points are either inside or outside the snake according to a binary scheme.

In the first stage of the active contours, we use a balloon force which aims at growing from the initial seed while the magnitude of the gradient is lower than a certain threshold (we must be cautious with this threshold to avoid growing beyond the limits of the region we want to segment). This can be expressed with the following PDE:

$$\frac{\partial u}{\partial t} = g\left(I\right) v \left\| \bigtriangledown u \right\|, \tag{12}$$

where $g\left(I\right)$ is the stopping function described in (2). This PDE can be used for both, expanding or contracting contours, depending on the sign of v. In order to discretize this expression, we consider the dilation and erosion operators (D_d and E_d, where d stands for discrete) as follows:

$$u^{n+1}\left(x\right) = \begin{cases} D_d u^n\left(x\right) & \text{if } g\left(I\right)\left(x\right) \geq t \text{ and } v > 0 \\ E_d u^n\left(x\right) & \text{if } g\left(I\right)\left(x\right) \geq t \text{ and } v < 0 \\ u^n\left(x\right) & \text{otherwise} \end{cases} \tag{13}$$

where t is a threshold to determine when the evolution must be stopped. As our intention consists in expanding from the seed point, we make use of the first case, i.e., dilation.

However, balloon forces by themselves cannot provide precise and satisfactory contours. Therefore, when we have approached the edges and the magnitude of the gradient starts increasing, two more terms are introduced. One of them is a regularizing term which aims at smoothing the edges and

Copyright (c) IARIA, 2013. ISBN: 978-1-61208-310-0

filling the holes of the segmentation, avoiding an extremely irregular contour. This is obtained by controlling the curvature of the contour as follows:

$$\frac{\partial u}{\partial t} = g\left(I\right)\left\|\bigtriangledown u\right\|\left(div\left(\frac{\bigtriangledown u}{\left\|\bigtriangledown u\right\|}\right)\right). \tag{14}$$

In order to implement this kind of regularization, we consider the SI_d and IS_d operators:

$$\begin{aligned}\left(SI_d u\right)\left(x\right) &= \sup_{S\in B}\left(\inf_{y\in x+hS} u\left(y\right)\right)\\ \left(IS_d u\right)\left(x\right) &= \inf_{S\in B}\left(\sup_{y\in x+hS} u\left(y\right)\right)\end{aligned} \tag{15}$$

where $\sup$ is the supremum or least upper bound and $\inf$ is the infimum or greatest lower bound (h is a scale factor). The base B is a set of 9 planes (since we work with a 3D image, we deal with 9 planes instead of the 4 lines used in [19] and [20]), which cover all the possible planes within the neighborhood of the point which is being considered. The combination of both operators generates a smoother contour by performing erosion and dilation processes as follows:

$$u^{n+1}\left(x\right) = \begin{cases}\left(SI_d \circ IS_d u^n\right)\left(x\right) & \text{if } g\left(I\right)\left(x\right) \geq t\\ u^n\left(x\right) & \text{otherwise}\end{cases} \tag{16}$$

Finally, the third term is an attraction term, similar to that described in Section II (second term in (6)), although, in this case, the levels are only two, i.e., inside and outside the contour (1 or 0), and the condition to expand, contract, or remain constant depends on the product of the gradient of the current snake and that of the stopping function g:

$$\frac{\partial u}{\partial t} = \bigtriangledown g\left(I\right) \bigtriangledown u, \tag{17}$$

which is discretized as follows:

$$u^{n+1}\left(x\right) = \begin{cases}1 & \text{if } \bigtriangledown u^n\left(x\right) \bigtriangledown g\left(I\right)\left(x\right) > 0 \\ & \quad \text{and } g\left(I\right)\left(x\right) \geq t\\ 0 & \text{if } \bigtriangledown u^n\left(x\right) \bigtriangledown g\left(I\right)\left(x\right) < 0 \\ & \quad \text{and } g\left(I\right)\left(x\right) \geq t\\ u^n\left(x\right) & \text{otherwise}\end{cases} \tag{18}$$

Since the first iterations are supposed to be quite far away from the final result, we start by applying only the balloon term to speed up the process, and then introduce the other two terms and combine all of them.

Figure 2 illustrates the result of applying these three types of snakes from a single point for the segmentation of the liver. Although it is a 3D segmentation, we show a single image as a sample. As observed, the segmentation is not completely satisfactory, since the balloon force has been stopped by the proximity of the edges, the smoothing term has rounded the contour and the attraction term has not been strong enough to fit the contour to the edges in all its segments. For this reason, the multiscale approach described in the next section has been introduced to refine the results.

Figure 2. Final contour obtained for the liver using the morphological snakes in an image belonging to a computed tomography.

V. Multiscale Active Contours

As explained in Section II, the value of σ determines how far the edges can be from the approximation to be reached. If the initial segmentation is too coarse, we need to use a high value of σ, but, as we approach the edges, it should be lower to prevent the contour from being too rounded and poorly defined. Using higher values in the first iterations and lower ones in the last steps works properly if the distance from the current approximation to the actual contour is homogeneous along the snake.

Since it is usual that some segments of the snake are far away from the actual contour, while others are already close to it, we use a multiscale implementation, considering higher values of σ in the most homogeneous regions and reducing it when the edges are nearby. This way, the scale varies not only across the iterations, but also from one region to another in the same iteration. However, it is computationally expensive to work simultaneously with a large number of different scales. Therefore, we use a combination of a reduced set of them in a single stopping/attraction term:

$$g\left(I\right) = \frac{1}{\sqrt{1+\alpha\sum_{i=0}^{n}\left(w_n\left\|\nabla I_{\sigma_n}\right\|^2\right)}}, \tag{19}$$

where the weights w_n depend on the magnitude of the gradient computed on the smoothed image.

In fact, we use four scales and four blending functions which determine their weights, with the constraint that the sum of all of them is 1 for every gradient value. In the most homogeneous regions, large scales have a higher weight. Therefore, further edges can be reached and the probability of being stopped by a local minimum is reduced. When the magnitude of the gradient increases, the weight of the small scales is also increased. As a consequence, the contour can be refined according to the more detailed information.

Figure 3 shows how this approach improves the result of the segmentation of the liver, the spleen, the liquid in the stomach and a vertebra. Although the images which are shown

Copyright (c) IARIA, 2013. ISBN: 978-1-61208-310-0

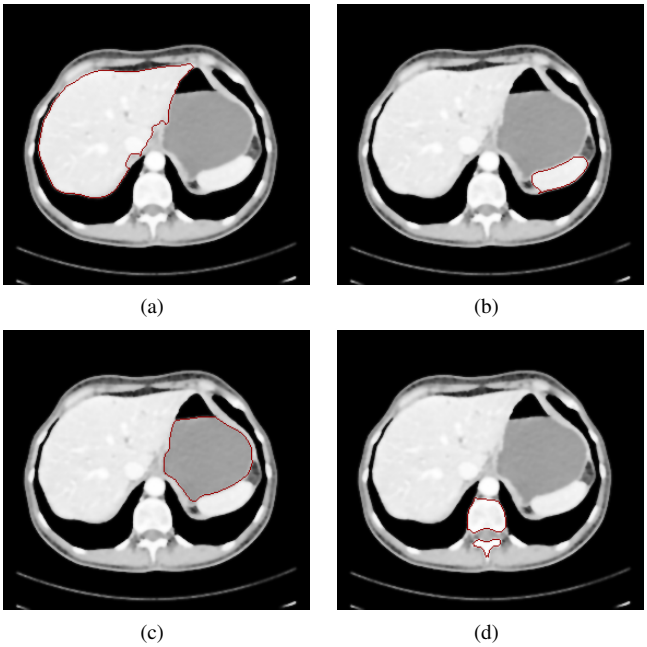

Figure 3. Final contours for: (a) the liver, (b) the spleen, (c) the liquid in the stomach, and (d) a vertebra, obtained after using the multiscale approach.

correspond to a single slice, the process is carried out in the whole tomography, adapting the snake according to the edges in all the slices. As observed, the combination of different scales, which simultaneously contribute to adjust the contour, allows adapting the evolution of the snake to the particular features of each region, instead of trying to find global values for the entire 3D image.

VI. Three-dimensional Processing and Contour Combination

The case of computed tomographies is a special one, since the 3D images are a combination of 2D images and, not only may the distance between the slices be different to the distance between the pixels in each 2D image, but it may also vary from one scan to another.

As mentioned above, we try to minimize human intervention and, at the same time, accelerate the process as much as possible. To this aim, when the seed point is selected to apply the morphological snakes, it is advisable to choose it in one of the central slices, in order to reduce the distance to the furthest edges in the volume. However, the thresholds for these morphological snakes must be chosen carefully to prevent the expansion from flooding other regions.

The final segmentation is given by a set of 3D points, which belong to the planes determined by the slices in the tomography. Figure 4 illustrates some slices of the 3D segmentation of the liver obtained from a single point in a computed tomography. Since the active contours are applied in the 3D image, a single point allows reaching the edges in the whole tomography. The balloon forces provide an initial volume, which is later refined by using the attraction, smoothing and multiscale terms.

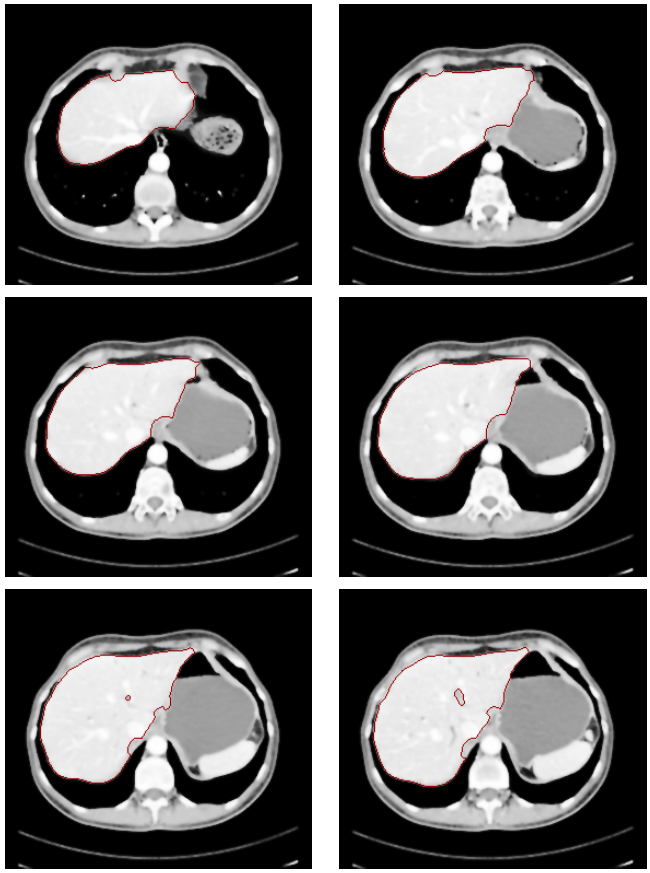

Figure 4. Final contours obtained for the liver in different slices of a computed tomography.

In order to represent the final segmentation in a more intuitive way, a triangulation process is applied by joining the 3D contour points. This allows building a 3D reconstruction of the region of interest and performing a further analysis when it is needed (e.g., measurements or shape analysis). Figure 5 illustrates the triangulation for a section of the liver. Figure 6 shows a 3D volume representation of the spleen.

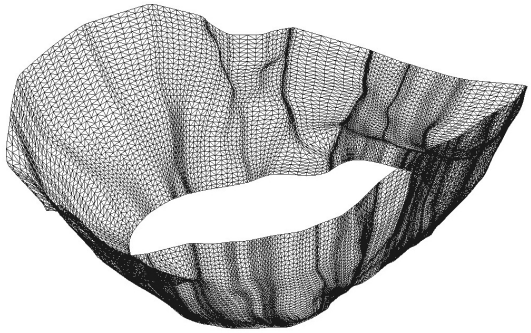

Figure 5. Triangulation of a section of the liver obtained from the 3D contour points.

Copyright (c) IARIA, 2013. ISBN: 978-1-61208-310-0

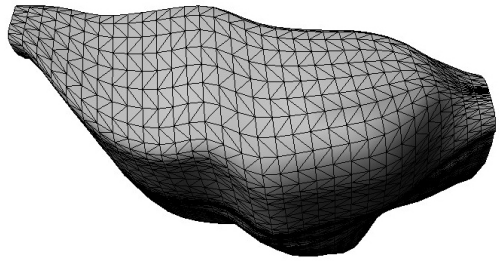

Figure 6. 3D representation of the spleen generated from the triangulation of the 3D segmentation.

As observed, introducing several scales in the active contours allows adapting the snake to the edges according to the rough and detailed information simultaneously, instead of predefining a single scale to work with.

VII. Conclusion and Future Work

In this paper, we have presented a method for obtaining a 3D segmentation of a region in a computed tomography by using an adaptive combination of different approaches for the active contours technique. Trying to tackle this problem with a single scheme would be very difficult, but adapting the contribution of the different terms to the needs of each stage and area allows obtaining quite satisfactory results. A combination of morphological operators, including balloon forces, regularizing filters and attraction terms, is used to extract a segmentation of the region of interest in a 3D image from a single seed point.

Furthermore, the use of different scales makes it possible to cope with those situations in which the contour is not uniformly close to the edges, accelerating the expansion in the most homogeneous regions and refining the contour when the final result is nearby. These multiscale active contours provide a framework to adapt the conditions of the snake to the particular area on which it is being computed. In this way, it is easier to deal with irregular edges and heterogeneous regions, since we make use of both, the coarse and the detailed information.

The results which have been obtained prove the efficiency of this approach and encourage its use for the semi-automatic analysis of medical images. The fact that the slices in the tomography are filtered and processed as a whole 3D image provides more consistent results and allows a further analysis for feature extraction, measurement or any other task which is required.

Future work includes accelerating the process and introducing some anatomical information which can help identify and distinguish the organs or tissues, as well as the application of this framework to the analysis of certain particular pathologies.

Acknowledgment

The authors would like to thank Dr. Patricia Alemán-Flores and Dr. Rafael Fuentes-Pavón from the Insular University Hospital of Gran Canaria for their collaboration in this research.

References

[1] L. Grady, “Random Walks for Image Segmentation,” IEEE Transactions on Pattern Analysis and Machine Intelligence, vol. 28, no. 11, 2006, pp. 1768-1783.

[2] T. Okada, K. Yokota, M. Hori, et al., “Construction of Hierarchical Multi-Organ Statistical Atlases and their Application to Multi-Organ Segmentation from CT Images,” Proc. MICCAI (1), 2008, pp. 502-509.

[3] C. Couprie, L. J. Grady, L. Najman, and H. Talbot, “Power watersheds: A new image segmentation framework extending graph cuts, random walker and optimal spanning forest,” Proc. ICCV, 2009, pp. 731-738.

[4] D. Kainmueller, T. Lange, and H. Lamecker, “Shape Constrained Automatic Segmentation of the Liver based on a Heuristic Intensity Model,” Proc. MICCAI Workshop on 3D Segmentation in the Clinic: A Grand Challenge, 2007, pp. 109-116.

[5] A. Beck and V. Aurich, “HepaTux–A Semiautomatic Liver Segmentation System,” Proc. MICCAI Workshop on 3D Segmentation in the Clinic: A Grand Challenge, 2007, pp. 225-233.

[6] V. Caselles, F. Catté, T. Coll, and F. Dibos, “A geometric model for active contours in image processing,” Numerische Mathematik, vol. 66, 1993, pp. 1-31.

[7] V. Caselles, R. Kimmel, and G. Sapiro, “Geodesic Active Contours, International Journal of Computer Vision,” vol. 22, no. 1, 1997, pp. 61-79.

[8] M. Kass, A. Witkin, and D. Terzopoulos, “Active Contour Models,” Proc. 1st International Conference on Computer Vision, 1987, pp. 259-268.

[9] T. Brox and J. Weickert, “Level set based image segmentation with multiple regions,” Pattern Recognition, Lecture Notes in Computer Science, vol. 3175, 2004, pp. 415-423.

[10] T. F. Chan, B. Y. Sandberg, and L. A. Vese, “Active contours without edges for vector-valued images,” J. Visual Communication and Image Representation, vol. 11, no. 2, 2000, pp. 130-141.

[11] D. Cremers, F. Tischhäuser, J. Weickert, and C. Schnörr, “Diffusion Snakes: Introducing Statistical Shape Knowledge into the Mumford-Shah Functional,” International Journal of Computer Vision, vol. 50, no. 3, 2002, pp. 295-313.

[12] N. Paragios and R. Deriche, “Geodesic active regions for supervised texture segmentation,” Proc. Internationl Conference on Computer Vision, 1999.

[13] C. Sagiv, N. A. Sochen, and Y. Y. Zeevi, “Integrated active contours for texture segmentation,” IEEE Transactions on Image Processing, vol. 15, no. 6, 2006, pp. 1633-1646.

[14] M. Alemán-Flores, L. Álvarez-León, and V. Caselles, “Texture-Oriented Anisotropic Filtering and Geodesic Active Contours in Breast Tumor Ultrasound Segmentation,” Journal of Mathematical Imaging and Vision, vol. 28, no. 1, 2007, pp. 81-97.

[15] M. Hernández and A. F. Frangi, “Geodesic active regions using nonparametric statistical regional description and their application to aneurysm segmentation from cta,” LNCS, vol. 3150, 2004, pp. 94-102.

[16] N. Paragios and R. Deriche, “Geodesic active contours and level sets for motion estimation and tracking,” Computer Vision and Image Understanding, vol. 97, no. 3, 2005, pp. 259-282.

[17] C. Lenglet, J. Campbell, M. Descoteaux, et al., “Mathematical Methods for diffusion MRI processing,” Neuroimage, vol. 45, no. 1, 2009, pp. 111-122.

[18] P. Perona and J. Malik, “Scale space and edge detection using anisotropic diffusion,” IEEE Transactions on Pattern Analysis and Machine Intelligence, vol. 12, 1990, pp. 629-639.

[19] L. Alvarez, L. Baumela, P. Márquez-Neila, and P. Henríquez, “A Real Time Morphological Snakes Algorithm,” Image Processing On Line, 2012.

[20] L. Alvarez, L. Baumela, P. Henríquez, and P. Márquez-Neila, “Morphological snakes,” Proc. CVPR, 2010, pp. 2197-2202.

Copyright (c) IARIA, 2013. ISBN: 978-1-61208-310-0